

RESEARCH

Open Access



Identifying the specific lipid biomarkers and *LYPLA1* as a novel candidate in intramuscular fat deposition of Erhualian pigs

Wenjing Meng¹, JiaYu Yan¹, Yuelei Zhao¹, Zijian Ye¹, Xiangfei Ma¹, Wei Wei¹, Jie Chen¹ and Lifan Zhang^{1*}

Abstract

Background Intramuscular fat (IMF) is a key determinant of meat quality enhancement in pigs. However, its correlation with subcutaneous fat (SCF) deposition presents a challenge. The precise regulation of IMF lipogenesis, without impacting SCF deposition, is a critical issue in the pig industry. To investigate this, our study examined the lipid profiles of longissimus dorsi (LD) muscle and subcutaneous adipose tissue in high IMF (IMFH) and low IMF (IMFL) Chinese Erhualian pigs using lipidomics techniques.

Results We identified 112 differentially abundant lipids (DALs) in the muscle and 101 DALs in the adipose tissue. Notably, 105 specific DALs associated with IMF, including various candidate markers like upregulated lipids of PS (19:2/18:1), TG (14:2/4:0/4:0), PS (17:1/18:2), FA(10:0) + COOH:(s), CL (20:4/18:2/18:2/18:2), and downregulated lipids of FA (20:4), SM (d43:5), TG (38:1/22:6), PC (22:3/20:3), and PC (18:2/24:8), were identified. These specific DALs were implicated in the regulation of linoleic, arachidonic, and alpha-linolenic acid metabolism, and choline metabolism in cancer. We further discovered that the lysophospholipase 1 (*LYPLA1*) gene promotes differentiation and lipid deposition of intramuscular pre-adipocytes by affecting the phosphatidylcholine (PC) content.

Conclusions Our findings identify specific lipids associated with IMF accumulation in both skeletal muscle and subcutaneous adipose depots, thereby offering valuable insights into the lipid composition of porcine IMF and new avenues for targeted IMF deposition.

Keywords Pig, Meat quality, Intramuscular fat, Lipidomics, *LYPLA1*

Background

Pork, as the most demanded meat globally, offers the advantages of excellent flavor, rich nutrients, and reasonable pricing. Consumers typically select pork based on immediate quality indicators such as meat color and odor, while flavor and palatability are crucial in determining repeat purchases. Previously, the Maillard reaction of water-soluble compounds during cooking has

been shown to contribute to basic saltiness and meat flavor. However, the degradation of intramuscular lipids imparts a distinctive fat aroma to the meat [1, 2]. Consequently, an increase in intramuscular fat (IMF) content can enhance the flavor and palatability of pork [3–5], underscoring the pivotal role of IMF in meat quality development. Among all lipids, triglycerides (TG) and phospholipids are the most prevalent lipid compounds. TG is a major storage lipid, and studies showed that *GPAT1* and *GPAT2*, which are key genes related to TG synthesis, have important effects on the IMF content of pigs [6, 7], whereas phospholipids, structural lipids forming the primary components of cell and organelle membranes [8, 9]. The lipolysis of phospholipids can influence

*Correspondence:

Lifan Zhang
lifanzhang@njau.edu.cn

¹ College of Animal Science and Technology, Nanjing Agricultural University, Nanjing 210095, China



© The Author(s) 2025. **Open Access** This article is licensed under a Creative Commons Attribution-NonCommercial-NoDerivatives 4.0 International License, which permits any non-commercial use, sharing, distribution and reproduction in any medium or format, as long as you give appropriate credit to the original author(s) and the source, provide a link to the Creative Commons licence, and indicate if you modified the licensed material. You do not have permission under this licence to share adapted material derived from this article or parts of it. The images or other third party material in this article are included in the article's Creative Commons licence, unless indicated otherwise in a credit line to the material. If material is not included in the article's Creative Commons licence and your intended use is not permitted by statutory regulation or exceeds the permitted use, you will need to obtain permission directly from the copyright holder. To view a copy of this licence, visit <http://creativecommons.org/licenses/by-nc-nd/4.0/>.

the formation of volatile flavor compounds during cooking [10, 11]. This highlights the significant influence of these lipids on meat flavor.

Meanwhile, there is a noted synergistic effect between IMF and subcutaneous fat (SCF) deposition, indicating that an increase in IMF contents often leads to heightened SCF deposition [12]. In the pig industry, excessive SCF deposition can lower the lean meat yield and rise the breeding costs of pigs [13]. Therefore, understanding the differences between IMF and SCF deposition is crucial for enhancing IMF contents without impacting SCF deposition. Numerous studies have identified genetic variations that specifically influence IMF deposition in pigs. For instance, different genotypes of the *SREBF1* gene in the muscle of Suta pigs have been linked to IMF content, rather than backfat thickness, a measure used for SCF deposition [14]. In a F₂ population crossbred between Korean native pigs and Landrace breeds, two out of nine single nucleotide polymorphisms (SNPs) were found to be exclusively related to IMF and not SCF deposition [15]. Similarly, in Duroc pigs, six SNPs were significantly associated with both IMF contents and backfat thickness, yet four of these SNPs were solely linked to IMF content [16]. However, little is currently known about the specific lipid composition of IMF in pigs.

Chinese Erhualian pigs are renowned for their high fertility and exceptional meat quality. Typically, the IMF content of this breed ranges from 2.5% to 5% at market weight, making it an ideal subject for studying IMF deposition in pigs. Consequently, this study utilized lipidomics to analyze the intramuscular and subcutaneous lipid compositions of high and low IMF content groups in Chinese Erhualian pigs. As this is the first attempt to compare the differences in lipid composition between IMF and SCF tissues, we aim to identify specific lipids and metabolic pathways or genes associated with IMF deposition. These findings offer comprehensive insights into potential lipid metabolites or new genes related to the specific adipogenesis of IMF and their corresponding pathways in pigs.

Methods

Animals

Chinese Erhualian pigs, approximately 270 days old, were sourced from the Changzhou Erhualian Pig Production Cooperation in Changzhou, Jiangsu, China. From a group with similar body weights, 10 and 11 pigs were selected for the high intramuscular fat (IMFH, 4.86% ± 0.57) and low intramuscular fat (IMFL, 2.70% ± 0.39) content groups, respectively. All pigs were reared under identical environmental conditions and fed a standard diet twice a day in compliance with the Chinese feeding standard for pigs (NY/T65-2004). In strict accordance with the

Chinese national standard for pig slaughtering (GB/T 17236–2019), the Erhualian pigs were electrically stunned and then exsanguinated at Ligang pig slaughtering center in Jiangyin, Jiangsu, China. Post-slaughter, approximately 20 g of the longissimus dorsi (LD) muscle and 4 g of SCF tissue were collected from each pig. Of these, about 4 g of LD muscle and 4 g of SCF tissues were immediately frozen in liquid nitrogen and subsequently transferred to an ultra-freezer at -80 °C for lipidomics and quantitative real-time RCR (qRT-PCR) analysis. The remaining LD muscle samples were preserved at 4 °C for assessing meat quality traits. All animal experiment procedures received approval from the Animal Ethics Committee of Nanjing Agricultural University (Approval No.20220318053).

Measurement of meat quality traits

The IMF contents of each sample was determined through the Soxhlet extraction method. The meat color L* (lightness), a* (redness), and b* (yellowness) values of the longissimus dorsi, were measured at 1 h and 24 h post-slaughter, respectively, using a chroma meter provided by Beijing Kemei Runda Instrument Equipment Co., Ltd, Beijing. Additionally, the shear force, an indicator of meat tenderness, was assessed 48 h after slaughter using a muscle tenderness meter (College of Engineering, Northeast Agricultural University). Backfat of shoulder, thoracolumbar junction, and lumbosacral joint was measured using an electronic vernier caliper. The average value of backfat in these three parts was taken as the average backfat thickness. The fatty acid (FA) composition of the longissimus dorsi was determined by gas chromatograph (GC7890, Shimadzu Corporation of Japan).

Lipid extraction

A total of 100 mg of muscle tissue from each individual was homogenized using a tissue grinder (model TS-24, Shanghai Jingxin Industrial Development Co., Ltd., Shanghai) and transferred to a glass tube with a Teflon-lined cap. To this tube, 0.75 mL of pre-cooled methanol was added and the mixture was vortexed. Subsequently, 2.5 mL of pre-cooled methyl tert-butyl ether (MTBE) was introduced, and the mixture was incubated at room temperature on a shaker for 1 h. Following this, 0.625 mL of mass spectrometry (MS)-grade water was added, and the samples were further incubated at room temperature for 10 min, then centrifuged at 1,000 g for 10 min. The upper organic phase was collected, and the lower phase was subjected to a second extraction using 1 mL of a solvent mixture (MTBE/methanol/water in a 10:3:2.5 ratio, v/v/v). The upper organic phase was collected again, enhancing lipid purity and improving extraction efficiency. The combined organic phases were dried and reconstituted in 100 µL of isopropanol for subsequent

UHPLC-MS/MS analysis. An equal volume of supernatant from each processed sample was mixed thoroughly to serve as quality control (QC) samples.

UHPLC-MS/MS analysis

UHPLC-MS/MS analysis was conducted using the Vanquish UHPLC system (Thermo Fisher Scientific, San Jose, CA, USA) and the Orbitrap Q Exactive™ HF mass spectrometer (Thermo Fisher Scientific, San Jose, CA, USA) at Novogene Co., Ltd. (Beijing, China). Samples were injected into the Thermo Accucore C30 chromatographic column with a linear gradient flow rate of 0.35 mL/min. The injection time and column temperature were set at 20 min and 40 °C, respectively. Mobile phase buffer A consisted of acetonitrile/water (6:4) with 10 mM ammonium acetate and 0.1% formic acid, while buffer B was isopropanol/acetonitrile (9:1) with 10 mM ammonium acetate and 0.1% formic acid. The solvent gradient was adjusted to 30%–70% buffer B over 2–11 min, 99% buffer B for 16 min, and returned to 30% buffer B at 18.1 min. The Q Exactive™ HF mass spectrometer operated with the following settings: sheath gas at 40 psi, sweep gas at 0 L/min, auxiliary gas rate at 10 L/min for positive and 7 L/min for negative ion mode, spray voltage at 3.5 kV, capillary temperature at 320 °C, heater temperature at 350 °C, S-lens RF level at 50, scan range from 114–1700 m/z, automatic gain control target at 3e6, normalized collision energy set at 22 eV, 24 eV, and 28 eV for both positive and negative ions, injection time at 100 ms, isolation window at 1 m/z, automatic gain control target at 2e5, and dynamic exclusion at 6 s.

Differential abundant lipid (DAL) identification

Principal component analysis (PCA), partial least squares discriminant analysis (PLS-DA), and orthogonal partial least squares discriminant analysis (OPLS-DA) were performed using MetaboAnalyst 5.0 (<https://www.metaboanalyst.ca>). Permutation tests were conducted via OPLS-DA, and variable importance in projection (VIP) scores were derived from both PLS-DA and OPLS-DA results. After base-2 logarithmic transformation of lipid metabolite data, Shapiro–Wilk tests for normality and Levene's tests for homogeneity of variances were conducted, followed by *P*-value calculation using the described statistical approaches: Student's *t*-test was used for normally distributed data with homogeneous variances; Welch's *t*-test for normal but heteroscedastic data; and Mann–Whitney *U* test for non-normal data. Fold changes (FC) values were calculated as the ratio of the mean value of each lipid compound in the IMFH group to that in the IMFL group. A lipid compound was defined as a DAL if it had a variable importance in projection (VIP) score greater than 1 from both PLS-DA and

OPLS-DA models, a *p*-value < 0.05, and a FC value > 1.2 or < 0.8. Volcano plots were generated using GraphPad Prism 9.0.

Pathway enrichment analysis

The metabolic pathways of the selected DALs were carried out on the NovoMagic platform of Novogene Co., Ltd (<https://magic-plus.novogene.com>). Specifically, the Kyoto Encyclopedia of Genes and Genomes (KEGG) pathway database was employed as the reference. A bioinformatics pipeline was built with Perl 5.18.2, and KEGG enrichment analysis used a hypergeometric test implemented in R 4.0.3. Subsequently, KEGG pathway maps were generated using Python 3.5.0. Pathways exhibiting *P*-value < 0.05 were designated as statistically significant.

Cell collection and differentiation of intramuscular pre-adipocytes

Three 7-day-old Erhualian piglets were humanely euthanized via intraperitoneal injection of pentobarbital sodium at a dosage of 50 mg/kg body weight, followed by aseptic exsanguination. Subsequently, intramuscular pre-adipocytes were collected from LD muscles isolated from these piglets, following the steps we previously reported [17]. Plasmids harboring *LYPLA1* (pcDNA3.1-*LYPLA1*) and small interfering RNA (siRNA) of *LYPLA1* (si-*LYPLA1*) were constructed separately. When the cells density reached 80%, pcDNA3.1-*LYPLA1* or si-*LYPLA1* was transfected with Lipofectamine 2000 kit (Invitrogen, Carlsbad, CA, USA) (Table S1). The cells were induced by induction medium for 4 d and fresh induction medium was replaced every other day. The components of induction medium contained 1 µg/mL insulin, 2 µg/mL dexamethasone, 1 µmol/L rosiglitazone, 5 nmol/L triiodothyronine, 100 µmol/L 3-isobutyl-1 methylxanthine, 125 µmol/L indomethacin, 1% penicillin–streptomycin, and 10% fetal bovine serum in Dulbecco's modified eagle's medium–high glucose (DMEM-HG) (Servicebio Technology Co., Ltd, Wuhan, China). The cells were then differentiated for 4 d in maintenance medium (1 µg/mL insulin, 1 µmol/L rosiglitazone, 5 nmol/L triiodothyronine, 1% penicillin–streptomycin, 10% fetal bovine serum in DMEM-HG); maintenance medium was replaced every other day.

qRT-qPCR assay

The total RNA of intramuscular pre-adipocytes or LD muscle tissues was extracted by using the Trizol reagent kit. Reverse transcription was conducted using the Hifair®II 1st Strand cDNA Synthesis SuperMix for the qPCR (Yeasen, Shanghai, China), followed by qRT-PCR with qPCR SYBR Green Master MIX (Abclonal, Wuhan, Hubei, China) on the QuantStudio™ 5 Real-Time

PCR System (Thermo Fisher Scientific, MA, USA). The expression levels of genes were measured using the $2^{-\Delta\Delta C_t}$ method. *GAPDH* was selected as an internal reference gene. All primers of genes used in qRT-PCR assay are listed in Table S1.

Oil red phenotype and triglyceride content determination

Intramuscular pre-adipocytes on 8 d of differentiation were washed with PBS and fixed with 4% paraformaldehyde for 30 min. After removing the paraformaldehyde, the cellular specimens were rinsed again with PBS. Subsequently, the accumulation of lipid droplets was visualized through oil red O staining for 30 min. Cell morphology was assessed using a Zeiss inverted microscope (Thornwood, NY, USA). Finally, the cells were decolorized with isopropanolyl and absorbance was measured at 510 nm to obtain the triglyceride content.

Determination of phosphatidylcholine (PC) content

The PC content of intramuscular pre-adipocytes was determined using a phosphatidylcholine ELISA kit (Nanjing Jiancheng Technology Co., Ltd, Nanjing, China) and measured at 450 nm absorbance.

Statistical analysis

Statistical analyses were performed using SPSS 17.0. Data normality and variance homogeneity were assessed via Shapiro–Wilk and Levene's tests, respectively. Two-group comparisons employed Student's *t*-test, Welch's *t*-test, or Mann–Whitney *U* test based on parametric assumptions, consistent with the *P*-value calculation in prior DAL identification. One-way analysis of variance and Tukey's test was used when comparing more than two groups. The data represented as mean \pm standard deviation (SD). $P < 0.05$ and $P < 0.01$ or 0.001 was indicated significant or highly significant differences, respectively.

Results

Phenotypic differences in meat quality between IMFH and IMFL pigs

As presented in Table 1, the IMF contents of the IMFH pigs was significantly higher than that of the IMFL group ($P < 0.001$). Meanwhile, there was no significant difference in body weight between these two groups ($P > 0.05$). Furthermore, the IMFH pigs exhibited significantly higher $L^*_{24\text{ h}}$ and $b^*_{24\text{ h}}$ values in meat color compared to the IMFL pigs ($P < 0.05$ or $P < 0.01$). In contrast, no significant differences were observed in $L^*_{1\text{ h}}$, $a^*_{1\text{ h}}$, $b^*_{1\text{ h}}$, $a^*_{24\text{ h}}$, shear force, and average back fat thickness between the IMFH and IMFL pigs ($P > 0.05$). Compared with IMFL group, IMFH pigs contained more saturated fatty acids (SFA, $P = 0.095$) and monounsaturated fatty acids (MUFA, $P < 0.05$), as well as less polyunsaturated fatty

acids (PUFA, $P < 0.001$). Among them, the contents of oleic acid of the IMFH pigs were significantly higher than that of the IMFL pigs ($P < 0.05$), whereas the contents of pentadecanoic acid, heptadecanoic acid, linoleic acid, α -linolenic acid, cis-11,14-eicosadienoic acid, and arachidonic acid of the IMFH pigs were significantly lower than that of the IMFL pigs ($P < 0.05$ or $P < 0.01/0.001$).

Characteristics of lipid compounds in the longissimus dorsi (LD) muscles of IMFH and IMFL pigs

A total of 1,159 lipid compounds were detected in the LD muscles across all samples, with 688 identified in positive ion mode and 471 in negative ion mode (Table S2). As depicted in Fig. 1A, B, glycerophospholipids (GP, 42.15%) were the most prevalent in positive ion mode, predominantly comprising phosphatidylcholine (PC, 22.67%), phosphatidylethanolamine (PE, 8.28%), phosphatidylserine (PS, 3.20%), lyso-phosphatidylcholine (LPC, 2.33%), phosphatidylinositol (PI, 1.60%), and phosphatidylglycerol (PG, 1.16%). Glycerolipids (GL, 39.40%) were the second most abundant, mainly consisting of triglyceride (TG, 28.20%) and diglyceride (DG, 10.47%). Sphingolipids (SP, 15.26%), including sphingomyelin (SM, 7.27%) and ceramide (Cer, 6.25%), were the third largest lipid class. Additionally, a minor proportion of fatty acids (FA, 2.76%) was also detected (Fig. 1A). In negative ion mode, the primary lipids were glycerophospholipids (GP, 87.47%), sphingolipids (SP, 8.92%), and fatty acids (FA, 3.61%) (Fig. 1E). The most abundant subclasses included PC (25.05%), PE (19.53%), cardiolipin (CL, 8.70%), PS (8.49%), PI (7.64%), Cer (4.88%), and PG (3.82%) (Fig. 1F). The PCA results showed that QC samples clustered together (Fig. 1C and G), demonstrating the stability and high quality of the lipid determination process. Furthermore, the OPLS-DA scatter plot revealed a clear separation between IMFH and IMFL pigs under both positive and negative ion modes (Fig. 1D and H).

Characteristics of lipid compounds in subcutaneous adipose tissues of IMFH and IMFL pigs

A total of 184 and 378 lipid compounds were identified in the subcutaneous adipose tissues of IMFH and IMFL pigs, respectively, when analyzed in positive and negative ion modes (Table S3). In the positive ion mode, the most abundant lipid was GP (57.07%), followed by GL (25.54%), SP (11.96%), and FA (5.43%) (Fig. S1A). The most abundant subcategories were PC (37.50%) and TG (16.85%) (Fig. S1B). In the negative ion mode, four types of lipids were detected: GP at 80.95%, SP at 11.38%, FA at 7.41%, and sterol (ST) at 0.26% (Fig. S1E). Within these, PC (25.40%), PE (22.49%), PS (11.11%), FA (7.41%), and SM (6.08%) were the subcategories with the highest contents (Fig. S1F). The results of PCA and OPLS-DA

Table 1 The phenotype of meat quality between IMFH and IMFL groups

Item	IMFH (n = 10)	IMFL (n = 11)	P value
Body weight (kg)	75.90 ± 6.36	74.29 ± 6.17	0.563
IMF content (%)	4.86 ± 0.57	2.70 ± 0.39***	< 0.001
L*1 h	45.25 ± 2.60	43.13 ± 2.82	0.090
a*1 h	6.54 ± 2.86	6.75 ± 4.51	0.705
b*1 h	10.95 ± 1.52	10.39 ± 2.04	0.489
L*24 h	50.36 ± 2.26	45.45 ± 3.53**	0.001
a*24 h	8.19 ± 2.72	7.26 ± 5.35	0.152
b*24 h	14.02 ± 1.76	11.63 ± 3.27	0.024
shear force 48 h (N)	33.45 ± 11.63	30.91 ± 11.23	0.617
Backfat of shoulder (mm)	36.94 ± 8.36	32.91 ± 5.77	0.220
Backfat of thoracolumbar junction (mm)	21.85 ± 4.69	17.97 ± 4.73	0.090
Backfat of lumbosacral joint (mm)	20.00 ± 3.67	18.47 ± 5.99	0.516
Average backfat thickness at three points (mm)	26.26 ± 5.26	23.12 ± 4.52	0.072
Caprylic acid	0.045 ± 0.065	0.059 ± 0.066	0.705
Capric acid	0.129 ± 0.085	0.151 ± 0.080	0.756
Lauric acid	0.095 ± 0.059	0.106 ± 0.058	0.665
Myristic acid	1.655 ± 0.331	1.554 ± 0.340	0.557
Pentadecanoic acid	0.035 ± 0.031	0.064 ± 0.029*	0.035
Palmitic acid	27.300 ± 1.742	25.850 ± 1.428	0.050
Heptadecanoic acid	0.238 ± 0.068	0.299 ± 0.053*	0.010
Stearic acid	14.290 ± 1.587	13.930 ± 1.505	0.592
Arachidic acid	0.283 ± 0.036	0.256 ± 0.049	0.189
SFA	44.071 ± 2.531	42.263 ± 2.180	0.095
Palmitoleic acid	3.501 ± 0.839	3.231 ± 0.704	0.432
Oleic acid	40.480 ± 3.603	36.930 ± 2.754*	0.019
Cis-11-Eicosenoic acid	0.735 ± 0.164	0.705 ± 0.134	0.973
MUFA	44.921 ± 3.719	40.864 ± 2.975*	0.012
Linoleic acid	8.479 ± 2.473	13.060 ± 2.330***	< 0.001
γ-linolenic acid	0.024 ± 0.036	0.034 ± 0.039	0.582
α-linolenic acid	0.355 ± 0.091	0.485 ± 0.109**	0.008
Cis-11,14-Eicosadienoic acid	0.330 ± 0.111	0.479 ± 0.087**	0.002
Cis-8,11,14-Eicosatrienoic acid	0.290 ± 0.176	0.386 ± 0.173	0.226
Arachidonic acid	1.107 ± 0.795	2.184 ± 1.194*	0.026
Cis-4,7,10,13,16,19-Docosahexaenoic	0.050 ± 0.063	0.093 ± 0.073	0.167
PUFA	10.636 ± 3.158	16.725 ± 3.275***	< 0.001

IMF Intramuscular fat, IMFH High intramuscular fat content population, IMFL Low intramuscular fat content population, SFA Saturated fatty acid, MUFA Monounsaturated fatty acid, PUFA Polyunsaturated fatty acid. Data are presented as mean ± SD (standard deviation)

* $P < 0.05$

** $P < 0.01$

*** $P < 0.001$

indicated that there was no marked separation between these two groups (Fig. S1C-D and S1G-H).

DALs identification between IMFH and IMFL pigs in the LD muscles

A total of 60 DALs were identified in the positive ion mode, including 28 GP, 21 GL, 9 SP, and 2 FA (Fig. 2A

and Table S4). In comparison with the IMFL pigs, 6 lipids were significantly upregulated, and 54 were significantly downregulated in the IMFH pigs (Fig. 2B and C). The upregulated lipids included DG (13:0/19:2), PE (38:7), SM (t39:1), TG (16:0/18:0/18:0), TG (10:0/18:0/18:1) and TG (14:2/4:0/4:0), while the downregulated lipids were primarily GP and GL. In the negative ion mode, 52 DALs

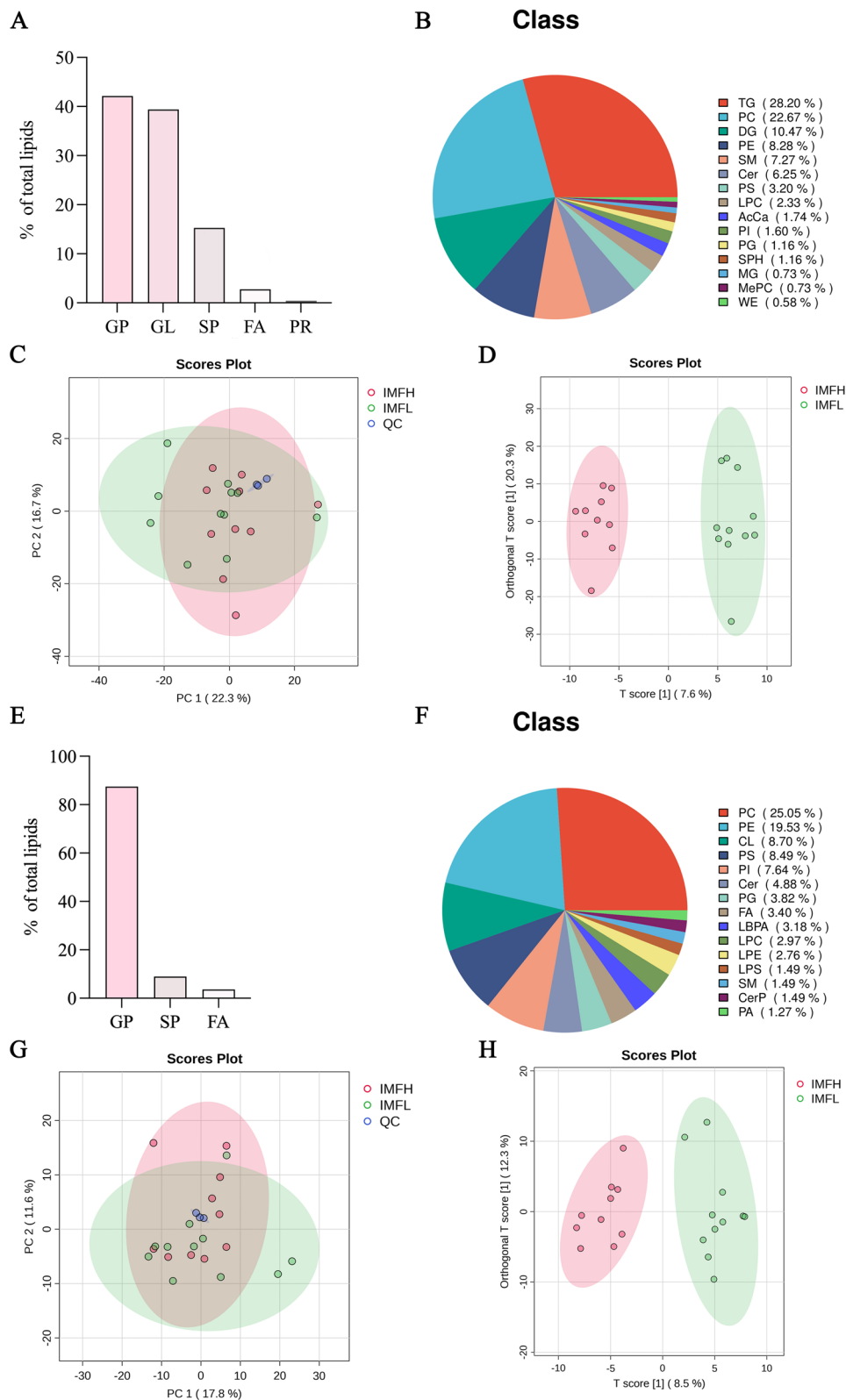


Fig. 1 Lipidomic analysis of LD muscles in IMFH and IMFL pigs. **A, E** Lipid classes in LD muscles under positive and negative ion modes. **B, F** Lipid subclasses in LD muscles under positive and negative ion modes. **C, G** Principal component analysis of the confirmed lipids in LD muscles under positive and negative ion modes. **D, H** Orthogonal partial least squares discriminant analysis of the confirmed lipids in LD muscles under positive and negative ion modes. $n = 10-11$ for each group

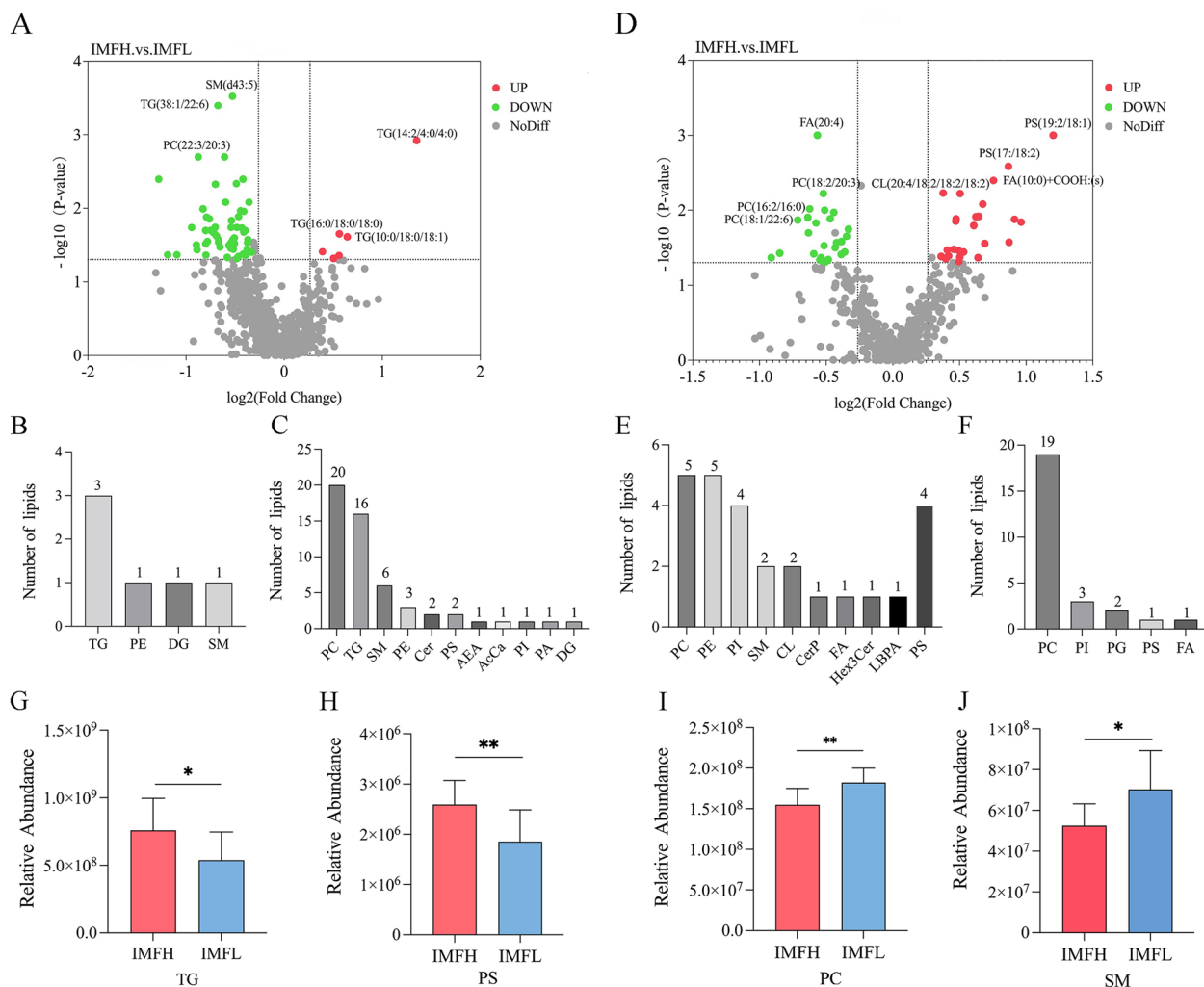


Fig. 2 Analysis of DALs of IMFH and IMFL in the LD muscles. **A, D** Volcano plot of DALs in positive and negative ion modes. **B, C** Upregulated and downregulated DALs in positive ion mode. **E, F** Upregulated and downregulated DALs in negative ion mode. **G–J** Summation of peak areas of DALs in different subclasses of IMFH and IMFL pigs. Data are presented as mean \pm SD. $n = 10–11$ for each group. * $P < 0.05$, ** $P < 0.01$

were identified, with 26 significantly upregulated and 26 downregulated in the IMFH group (Fig. 2D and Table S5). This group consisted of 21 GP, 4 SP, and 1 FA upregulated lipids, and the downregulated lipids included 25 GP and 1 FA (Fig. 2E and F). Further analysis of the peak areas of DALs within the same subclass revealed that the total TG content and PS in IMFH was significantly higher than in IMFL ($P < 0.05$ or $P < 0.01$) (Fig. 2G and H), despite the lower number of upregulated TGs compared to the number of downregulated TGs in IMFH (Fig. 2B and C). Inversely, the contents of PC and SM in the IMFH pigs were significantly reduced compared to the IMFL pigs ($P < 0.05$ or $P < 0.01$) (Fig. 2I and J).

Identification of specific DALs related to IMF

To explore whether DALs in the LD muscle influence SCF deposition, we compared these DALs in SCF tissues

between IMFH and IMFL pigs. We found 40 DALs in positive ion mode and 61 DALs in negative ion mode exhibiting significant differences between these two groups (Tables S6 and S7). Of these, 5 DALs in positive ion mode and 2 in negative ion mode were common to both groups. These 7 lipids displayed a consistent trend of change in both LD and SCF tissues in IMFH and IMFL pigs (Fig. 3A and B). Excluding these lipids, there were 55 specific DALs in LD muscle tissue in positive ion mode and 50 in negative ion mode. The five most significantly upregulated lipids in IMFH pigs were PS (19:2/18:1), TG (14:2/4:0/4:0), PS (17:1/18:2), FA (10:0) + COOH:(s), and CL (20:4/18:2/18:2/18:2) (Fig. 3C–G). In contrast, the five most significantly downregulated lipids in IMFH pigs were FA (20:4), SM (d43:5), TG (38:1/22:6), PC (22:3/20:3), and PC (18:2/24:8) (Fig. 3H–L and Tables S4–S5).

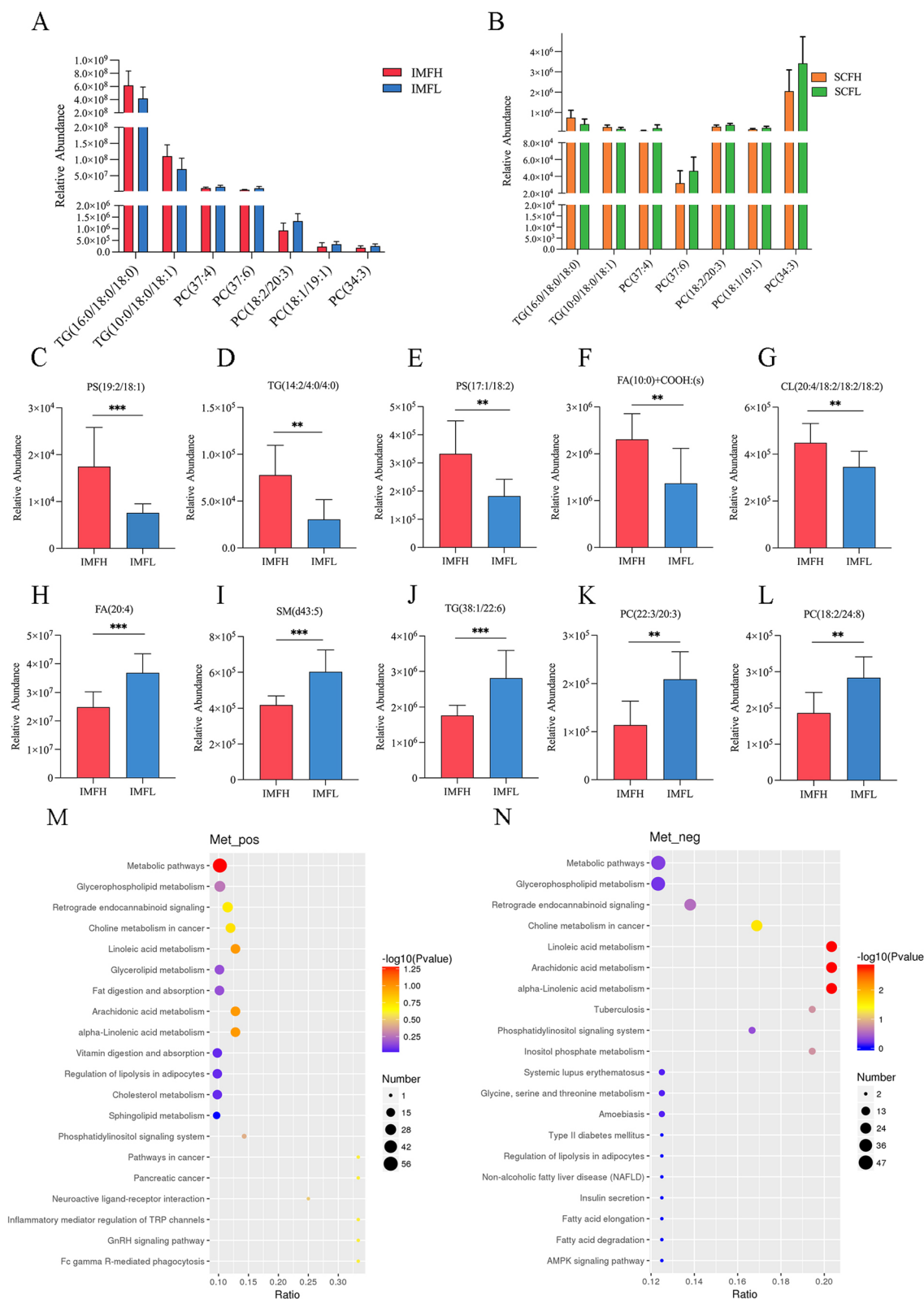


Fig. 3 Analysis of specific DALs in LD muscles. **A, B** DALs shared by IMF and SCF tissues. **C-G** Five most significantly upregulated DALs in IMFH pigs compared with IMFL pigs. **H-L** Five most significantly downregulated DALs in IMFH pigs compared with IMFL pigs. **M, N** KEGG enrichment analysis of DALs under positive and negative ion modes. The color represents $-\log_{10} p$ -value, while the size represents the number of DALs in the corresponding pathway. Data are presented as mean \pm SD. $n = 10-11$ for each group. $**P < 0.01$, $***P < 0.001$

Pathway analysis of specific DALs related to IMF

KEGG enrichment analysis revealed that the specific DALs associated with IMF primarily engage in metabolic pathways in positive ion mode (Fig. 3M, Table S8). Conversely, DALs in negative ion mode were significantly involved in linoleic acid metabolism, arachidonic acid metabolism, alpha-linolenic acid metabolism, and choline metabolism in cancer (Fig. 3N, Table S9).

Expression levels of *LYPLA1* associated with IMF deposition

Because 24 of the 26 (92%) unique DALs enriched in these above four metabolic pathways of negative ion mode belong to PC (Table S9), five genes related to PC metabolism, including *CHKA*, *LYPLA1*, *PEMT*, *PLA2G16*, and *PTDDSI*, were selected using qRT-PCR analysis between IMFH and IMFL pigs. As shown in Fig. 4A, only the expression of *LYPLA1* was significantly higher in IMFH pigs than in IMFL pigs ($P < 0.01$). During the differentiation process of intramuscular pre-adipocytes, the level of *LAPLA1* began to rise on day 2 of induction differentiation, reached its peak on day 4 and was significantly higher than that on day 0 ($P < 0.05$) (Fig. 4B).

Overexpression of *LYPLA1* promotes lipid deposition while reducing the PC content in intramuscular pre-adipocytes

When treating pcDNA3.1-*LYPLA1* for 48 h, the data demonstrated that the overexpression efficiency of *LYPLA1* was highly significant ($P < 0.001$) (Fig. 5A). After inducing differentiation for 8 d, overexpression of *LYPLA1* significantly up-regulated the levels of adipogenic markers *PPARG* and *FABP4* ($P < 0.01$; Fig. 5B and C) and triglycerides ($P < 0.01$; Fig. 5D and E), and down-regulated the levels of PC ($P < 0.05$; Fig. 5F).

Interference of *LYPLA1* inhibits lipid deposition while enhancing the PC content in intramuscular pre-adipocytes

When treating si-*LYPLA1* for 48 h, the interference efficiency of *LYPLA1* was significant ($P < 0.001$; Fig. 6A). After inducing differentiation for 8 d, interference of *LYPLA1* significantly down-regulated the levels of adipogenic markers *PPARG* and *FABP4* ($P < 0.05$ or $P < 0.01$; Fig. 6B and C) and triglycerides ($P < 0.01$; Fig. 6D and E), and up-regulated the levels of PC ($P < 0.01$; Fig. 6F).

Discussion

In this study, our data indicated that only the IMF, L*24 h, and b*24 h values were significantly higher in the IMFH group compared to the IMFL group (Table 1). This aligns with findings from a previous study [18], which observed that Ningxiang pigs with high IMF content at 24 h post-slaughter exhibited increased brightness and yellowness in the LD muscle. Since the L and b values represent meat color brightness and yellowness respectively, our results support the notion that higher IMF content may be associated with brighter, more yellow meat colors. Additionally, a previous study has shown that IMF is positively correlated with oleic acid content and negatively correlated with linoleic acid and PUFA content [19], which is similar to our data, suggesting that these FA might play an important role in IMF deposition of pigs (Table 1). Actually, the thermal oxidation of oleic acid can promote the formation of aldehydes, which have a pleasant fatty and oily odor, whereas the thermal oxidation of linoleic acid forms substances that may produce unpleasant odors at higher concentrations [20]. Compared with IMFL pigs, IMFH pigs had higher levels of oleic acid and simultaneously possessed lower levels of linoleic acid, indicating that the meat flavor of individuals from the IMFH group are better than that of IMFL pigs.

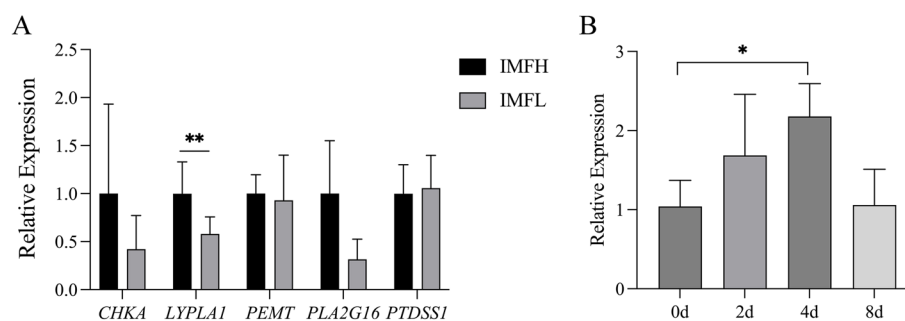


Fig. 4 The mRNA expression of genes related to PC metabolism between IMFH and IMFL pigs or the differentiation process of intramuscular pre-adipocytes. **A** The mRNA expression of *CHKA*, *LYPLA1*, *PEMT*, *PLA2G16*, and *PTDDSI* between IMFH and IMFL pigs. $n = 10-11$ for each group. **B** The mRNA expression of *LYPLA1* at different stages of differentiation in intramuscular pre-adipocytes. Data are presented as mean \pm SD. * $P < 0.05$, ** $P < 0.01$

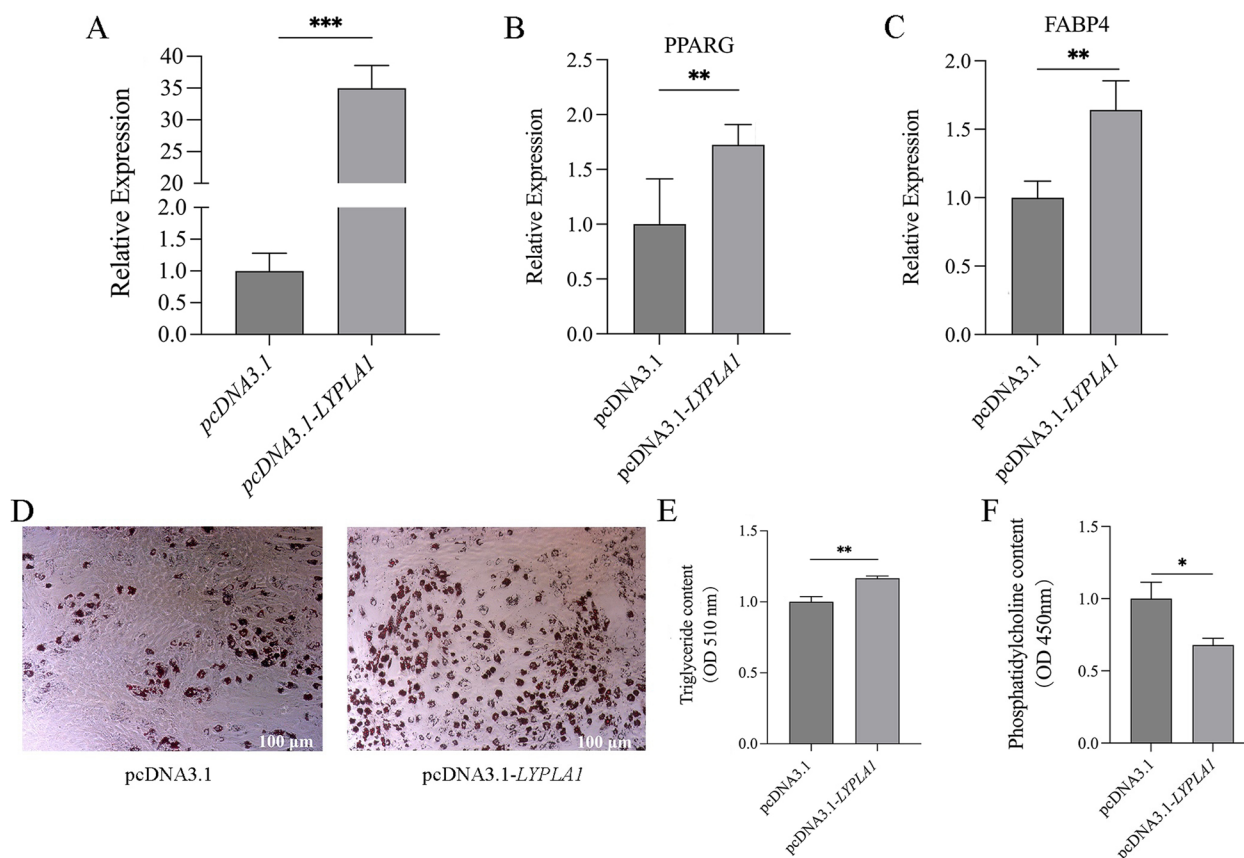


Fig. 5 Overexpression of *LYPLA1* promotes lipid deposition in intramuscular pre-adipocytes. **A** The mRNA levels of *LYPLA1* in pre-adipocytes treated with pcDNA3.1 or pcDNA3.1-*LYPLA1* for 48 h. **B, C** The mRNA levels of *PPARG* and *FABP4* in pre-adipocytes treated with pcDNA3.1 or pcDNA3.1-*LYPLA1* for 8 d. **D, E** Oil Red phenotypic (D) and triglyceride content (E) in pre-adipocytes treated with pcDNA3.1 or pcDNA3.1-*LYPLA1* for 8 d. **F** Phosphatidylcholine (PC) content in pre-adipocytes treated with pcDNA3.1 or pcDNA3.1-*LYPLA1* for 8 d. Data are presented as mean \pm SD. $n=3$ for each group. * $P < 0.05$, ** $P < 0.01$, *** $P < 0.001$

To identify specific DALs related to IMF, we conducted a lipidomics analysis on LD muscle and SCF tissues from both IMFH and IMFL groups. Our analysis revealed that IMF contained more TG, CL, and PI and less PC, SM, and FA than that of SCF tissues in positive and negative ion mode (Fig. 1B and 1E; Fig. S1B and S1F). Notably, only 7 DALs were common to both LD and SCF tissues across the two groups (Fig. 3A-B), indicating significant differences in lipid composition between IMF and SCF. Upon excluding these common DALs, we found that specific DALs related to IMF predominantly included TG, PC, PE, PI, PS, and SP (Fig. 2B-F; Tables S4-S5). Furthermore, the total contents of these differential TGs were significantly higher in the IMFH group than in the IMFL group (Fig. 2G). This is consistent with previous studies on Hu sheep and Beijing Heilium pigs, where individuals with higher IMF had greater TG and DG contents compared to those with lower IMF [21, 22]. These parallels suggest that variations in TG content might be a key factor influencing differences in IMF deposition in pigs.

PC and PE stand out as the most predominant phospholipids within mammalian cell and organelle membranes [23, 24]. On one hand, the increase of PE on the surface of lipid droplets promotes the merging of small lipid droplets to form large ones. On the other hand, the addition of PC to lipid droplets reduces the relative content of PE, thereby influencing droplet fusion [25, 26]. In this study, we identified 44 types of PC among the DALs, with 39 showing a downward trend in the IMFH group (Table S4-S5). Notably, two of the five most significantly downregulated lipids were PC (22:3/20:3) and PC (18:2/24:8) (Fig. 3K-L). This finding aligns with another study [27], which reported that Laiwu pigs, known for higher IMF, had more downregulated PCs compared to Yorkshire pigs. In contrast, of the 9 types of PE identified as DALs, 6 exhibited an upward trend in the IMFH group (Tables S4-S5), supporting the idea that IMF deposition may be inversely proportional to PC content and directly proportional to PE content. In animal adipose tissue, compared to PC and PE, the content of PS is

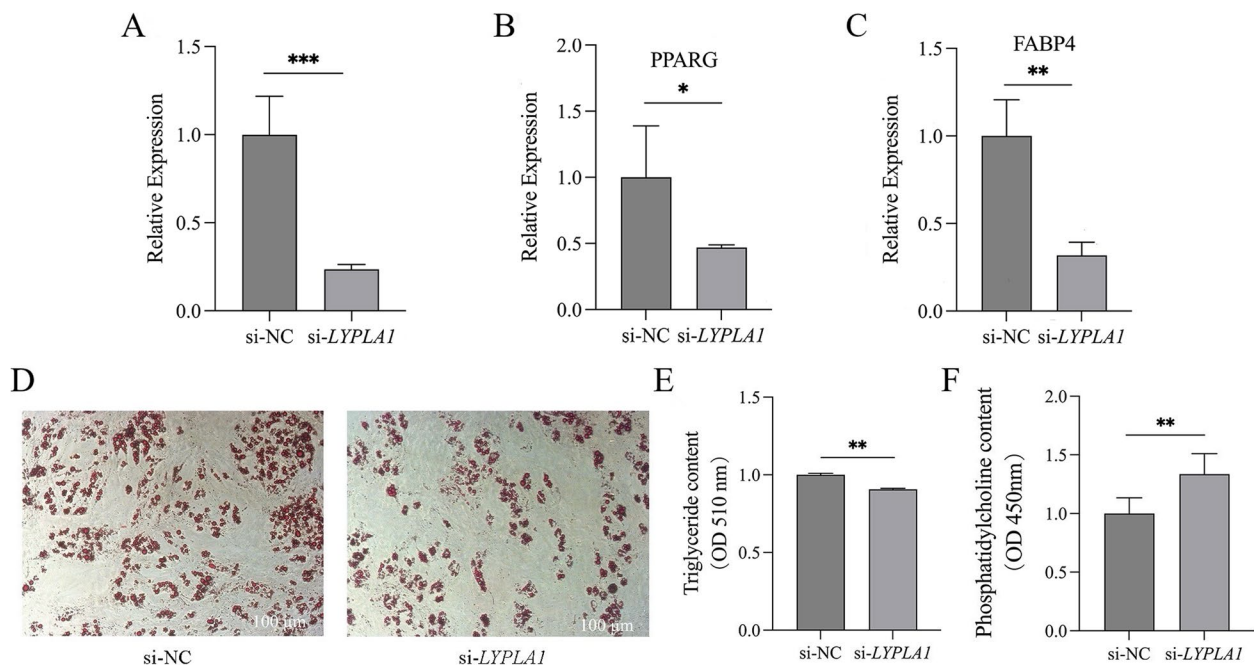


Fig. 6 Interference of *LYPLA1* inhibits lipid deposition in intramuscular pre-adipocytes. **A** The mRNA level of *LYPLA1* in pre-adipocytes treated with si-NC or si-*LYPLA1* for 48 h. **B, C** The mRNA levels of *PPARG* and *FABP4* in pre-adipocytes treated with si-NC or si-*LYPLA1* for 8 d. **D, E** Oil Red phenotype (**D**) and triglyceride content (**E**) in pre-adipocytes treated with si-NC or si-*LYPLA1* for 8 d. **F** PC content in pre-adipocytes treated with si-NC or si-*LYPLA1* for 8 d. Data are presented as mean \pm SD. $n=3$ for each group. * $P < 0.05$, ** $P < 0.01$, *** $P < 0.001$

lower, but it is crucial for the activation of many enzymes [28, 29]. A total of 24 differential PS were found in Xidu black pigs, all of which were significantly upregulated in the high IMF group [30]. In our study, 7 different types of PS were found in IMFH and IMFL (Fig. 2C-F), among which PS (19:2/18:1), PS (17:1/18:2), PS (17:1/20:3), and PS (18:0/19:2) were significantly upregulated in IMFH (Tables S5). And in the statistical analysis of the peak areas of these 7 PS, it was found that the content of PS in IMFH was significantly higher than that in IMFL (Fig. 2H). This suggests that PS may promote the deposition of IMF in Erhualian pigs. Additionally, in animal cells, CL is almost exclusively found in the inner membrane of mitochondria and plays a crucial role in regulating mitochondrial function [31–33]. In our study, CL (20:4/18:2/18:2/18:2) and CL (22:6/16:1/16:1/18:2) were found to be significantly upregulated in the IMFH group (Table S5), suggesting that muscles of IMFH individuals may have higher levels of mitochondrial respiratory function. However, further research is needed to investigate the specific mechanisms of CL in mitochondrial metabolism in pigs.

As the third largest category of lipids in the LD muscles of pigs, SP have been demonstrated to play a significant role in cellular functions and pathology, including cell growth, senescence, immune responses, and inflammatory processes [5, 34]. In our study, we found that

the contents of SM, a subclass of SP, were significantly lower in the IMFH group compared to the IMFL group (Fig. 2). Nine types of SM among the DALs were identified between IMFH and IMFL groups, among which SM (d43:5), SM (t40:3), SM (t40:6), SM (t38:1), SM (t42:6), and SM (d42:3) were significantly downregulated in the IMFH group (Tables S4-S5). This finding aligns with results from studies on Laiwu pigs, where individuals with higher IMF also exhibited notably lower SM levels compared to those with lower IMF [5]. Additionally, comparisons between different pig breeds revealed higher SM levels in Large White pigs, which typically have lower IMF content, as opposed to Jianhe White Xiang pigs with higher IMF content [35]. Thus, our data contribute new evidence suggesting that SM may influence the deposition of IMF in pigs.

KEGG enrichment analysis revealed that the DALs were primarily involved in linoleic acid metabolism, arachidonic acid metabolism, alpha-linolenic acid metabolism, and choline metabolism in cancer in negative ion mode (Fig. 3N). Interestingly, PC was found to be the main lipid involved in these four metabolic pathways (Table S9). Therefore, we further detected the expression of PC metabolism-related genes between IMFH and IMFL pigs and discovered that only *LYPLA1* showed a significant difference between these two groups. As a key regulatory factor in the decomposition of PC, *LYPLA1*

plays an important role in maintaining lipid homeostasis and membrane lipid composition in cells. A genome-wide association analysis in beef cattle found that *LYPLA1* was closely related to carcass weight and related characteristics [36]. In this study, we found that levels of *LYPLA1* in IMFH pigs were significantly higher than those in IMFL pigs. Overexpression of *LYPLA1* promoted the intracellular lipid accumulation while reducing PC content, whereas interference with *LYPLA1* decreased the intracellular lipid accumulation and simultaneously enhanced PC content, indicating that *LYPLA1* positively regulates IMF deposition. The negative correlation between PC content and IMF deposition was observed in Fig. 2I; these data suggested that *LYPLA1* may affect IMF deposition by altering intracellular PC content. So far, little is known about the exact function of *LYPLA1* in IMF deposition. Here our data provides first-hand evidence that *LYPLA1* can regulate the adipogenesis of porcine IMF.

Conclusion

In summary, this study offers a comprehensive overview of the lipid metabolite composition of IMF and SCF in pigs. Crucially, we identified specific lipids associated with IMF deposition in both skeletal muscle and subcutaneous adipose depots and their corresponding metabolic pathways. Besides, we further discovered that *LYPLA1* can serve as a novel candidate for affecting IMF adipogenesis. Our findings not only enhance the understanding of lipid composition in different body parts, but also propose potential biomarkers and gene for the targeted deposition of IMF in pigs. However, the limitations inherent in this study, primarily stemming from a restricted sample size, may compromise key parametric assumptions (e.g., normality and variance homogeneity) and thereby potentially undermine the statistical power of the analysis. Future investigations employing expanded sample sizes would allow for enhanced statistical power to enable more precise detection of lipidomic alterations.

Abbreviations

IMF	Intramuscular fat
SCF	Subcutaneous fat
LD	Longissimus dorsi
IMFH	High intramuscular fat population
IMFL	Low intramuscular fat population
DAL	Differentially abundant lipid
LYPLA1	Lysophospholipase 1
qRT-PCR	Quantitative real-time RCR
FA	Fatty acid
MTBE	Methyl tert-butyl ether
MS	Mass spectrometry
siRNA	Small interfering RNA
DMEM-HG	Dulbecco's modified eagle's medium-high glucose
SD	Standard deviation
GP	Glycerophospholipid
PC	Phosphatidylcholine
PE	Phosphatidylethanolamine
PS	Phosphatidylserine

LPC	Lyso-phosphatidylcholine
PI	Phosphatidylinositol
PG	Phosphatidylglycerol
GL	Glycerolipid
TG	Triglyceride
DG	Diglyceride
SP	Sphingolipid
SM	Sphingomyelin
Cer	Ceramide
CL	Cardiolipin
KEGG	Kyoto encyclopedia of genes and genomes
SFA	Saturated fatty acid
MUFA	Monounsaturated fatty acid
PUFA	Polyunsaturated fatty acid

Supplementary Information

The online version contains supplementary material available at <https://doi.org/10.1186/s12864-025-11611-z>.

Additional file 1: Table S1 Information of primer for RT-qPCR. Table S2 Lipid identification of LD muscles in IMFH and IMFL groups using lipidomics. Table S3 Lipid identification of SCF tissues in IMFH and IMFL groups using lipidomics. Table S4 DALs identification of LD muscles between IMFH and IMFL groups in positive ion mode. Table S5 DALs identification of LD muscles between IMFH and IMFL groups in negative ion mode. Table S6 DALs identification of SCF tissues between IMFH and IMFL groups in positive ion mode. Table S7 DALs identification of SCF tissues between IMFH and IMFL groups in negative ion mode. Table S8 KEGG enrichment analysis of DALs in LD muscles of IMFH and IMFL groups under positive ion mode. Table S9 KEGG enrichment analysis of DALs in LD muscle of IMFH and IMFL groups under negative ion mode. Fig. S1 Lipidomic analysis of SCF tissues in IMFH and IMFL groups. (A, E) Lipid classes in SCF tissues under positive and negative ion modes. (B, F) Lipid subclasses in SCF tissues under positive and negative ion modes. (C, G) Principal component analysis of lipids in SCF tissues under positive and negative ion modes. (D, H) Orthogonal partial least squares discriminant analysis of lipids in SCF tissues under positive and negative ion modes. $n = 10-11$ for each group.

Acknowledgements

Not applicable.

Authors' contributions

LZ conceived and designed the experiments. WM performed the experiments. WM, JY, and YZ analyzed the data. ZY, XM, WW, and JC participated in the collection of samples. WM and LZ wrote the manuscript. All authors read and approved the final manuscript.

Funding

This work was supported by the Biological Breeding-National Science and Technology Major Project (2023ZD04069), the National Natural Science Foundation of China (32472881), and the Accurate Identification Project of Livestock and Poultry Germplasm Resources (202114).

Data availability

The datasets used and/or analyzed during the current study are available from the corresponding author on reasonable request. All lipidomics data can be found in the Supplementary Table S2 and S3.

Declarations

Ethics approval and consent to participate

Not applicable.

Consent for publication

Not applicable.

Competing interests

The authors declare no competing interests.

Received: 18 October 2024 Accepted: 17 April 2025
Published online: 25 April 2025

References

- Bassam SM, Noleto-Dias C, Farag MA. Dissecting grilled red and white meat flavor: Its characteristics, production mechanisms, influencing factors and chemical hazards. *Food Chem.* 2022;371:131–139.
- Yang XL, Pei ZY, Du WB, Xie JC. Characterization of volatile flavor compounds in dry-rendered beef fat by different solvent-assisted flavor evaporation (SAFE) combined with GC-MS, GC-O, and OAV. *Foods.* 2023;12(17):3162.
- Ma QS, Kou XY, Yang YY, Yue YS, Xing WH, Feng XH, Liu GQ, Wang CF, Li Y. Comparison of lipids and volatile compounds in Dezhou donkey meat with high and low intramuscular fat content. *Foods.* 2023;12(17):3269.
- Ros-Freixedes R, Sadler LJ, Onteru SK, Smith RM, Young JM, Johnson AK, Lonergan SM, Huff-Lonergan E, Dekkers JCM, Rothschild MF. Relationship between gilt behavior and meat quality using principal component analysis. *Meat Sci.* 2014;96(1):264–9.
- Wang LY, Zhao XY, Liu SQ, You WJ, Huang YQ, Zhou YB, Chen WT, Zhang S, Wang JY, Zheng QK, et al. Single-nucleus and bulk RNA sequencing reveal cellular and transcriptional mechanisms underlying lipid dynamics in high marbled pork. *Npj Sci Food.* 2023;7(1):23.
- Mitka I, Ropka-Molik K, Tyra M. Functional analysis of genes involved in glycerolipids biosynthesis (GPAT1 and GPAT2) in pigs. *Animals-Basel.* 2019;9(6):308.
- Mitka I, Ropka-Molik K, Tyra M. Association between single nucleotide polymorphisms in GPAT1 locus and pork quality in pigs. *Meat Sci.* 2020;162:108045.
- McMaster CR. From yeast to humans - roles of the Kennedy pathway for phosphatidylcholine synthesis. *FEBS Lett.* 2018;592(8):1256–72.
- Yi WZ, Huang QX, Wang YZ, Shan TZ. Lipo-nutritional quality of pork: The lipid composition, regulation, and molecular mechanisms of fatty acid deposition. *Anim Nutr.* 2023;13:373–85.
- Tatijaborworntham N, Oz F, Richards MP, Wu HZ. Paradoxical effects of lipolysis on the lipid oxidation in meat and meat products. *Food Chem X.* 2022;14:100317.
- Tejeda JF, Gandemer G, Garcia C, Viau M, Antequera T. Contents and composition of individual phospholipid classes from biceps femoris related to the rearing system in Iberian pig. *Food Chem.* 2021;338:128102.
- Feng H, Yousuf S, Liu TY, Zhang XX, Huang WL, Li A, Xie LL, Miao XY. The comprehensive detection of miRNA and circRNA in the regulation of intramuscular and subcutaneous adipose tissue of Laiwu pig. *Sci Rep-Uk.* 2022;12(1):16542.
- Wu WJ, Zhang DW, Yin YJ, Ji M, Xu K, Huang X, Peng YJ, Zhang J. Comprehensive transcriptomic view of the role of the LGALS12 gene in porcine subcutaneous and intramuscular adipocytes. *BMC Genomics.* 2019;20:509.
- Chen J, Yang XJ, Xia D, Chen J, Wegner J, Jiang Z, Zhao RQ. Sterol regulatory element binding transcription factor 1 expression and genetic polymorphism significantly affect intramuscular fat deposition in the longissimus muscle of Erhualian and Suta pigs. *J Anim Sci.* 2008;86(1):57–63.
- Lee KT, Byun MJ, Kang KS, Hwang H, Park EW, Kim JM, Kim TH, Lee SH. Single nucleotide polymorphism association study for backfat and intramuscular fat content in the region between SW2098 and SW1881 on pig chromosome 6. *J Anim Sci.* 2012;90(4):1081–7.
- Zhang Z, Zhang Z, Oyelami FO, Sun H, Xu Z, Ma P, Wang Q, Pan Y. Identification of genes related to intramuscular fat independent of backfat thickness in Duroc pigs using single-step genome-wide association. *Anim Genet.* 2021;52(1):108–13.
- Tian Y, Zhao YL, Yu WS, Melak S, Niu YF, Wei W, Zhang LF, Chen J. ACAT2 is a novel negative regulator of pig intramuscular preadipocytes differentiation. *Biomolecules.* 2022;12(2):237.
- Chen JY, Chen FM, Lin X, Wang YD, He JH, Zhao YR. Effect of excessive or restrictive energy on growth performance, meat quality, and intramuscular fat deposition in finishing Ningxiang pigs. *Animals-Basel.* 2021;11(1):27.
- Zhang YF, Zhang JJ, Gong HF, Cui LL, Zhang WC, Ma JW, Chen CY, Ai HS, Xiao SJ, Huang LS, et al. Genetic correlation of fatty acid composition with growth, carcass, fat deposition and meat quality traits based on GWAS data in six pig populations. *Meat Sci.* 2019;150:47–55.
- Van Ba H, Ryu KS, Lan NTK, Hwang I. Influence of particular breed on meat quality parameters, sensory characteristics, and volatile components. *Food Sci Biotechnol.* 2013;22(3):651–8.
- Li J, Zhang JQ, Yang YY, Zhu JW, He WZ, Zhao QY, Tang CH, Qin YC, Zhang JM. Comparative characterization of lipids and volatile compounds of Beijing Heilium and Laiwu Chinese black pork as markers. *Food Res Int.* 2021;146:110433.
- Li J, Yang YY, Tang CH, Yue SN, Zhao QY, Li FD, Zhang JM. Changes in lipids and aroma compounds in intramuscular fat from Hu sheep. *Food Chem.* 2022;383:132611.
- Gibellini F, Smith TK. The Kennedy pathway—De novo synthesis of phosphatidylethanolamine and phosphatidylcholine. *IUBMB Life.* 2010;62(6):414–28.
- van der Veen JN, Kennelly JP, Wan S, Vance JE, Vance DE, Jacobs RL. The critical role of phosphatidylcholine and phosphatidylethanolamine metabolism in health and disease. *BBA-Biomembranes.* 2017;1859(9):1558–72.
- Guo Y, Walther TC, Rao M, Stuurman N, Goshima G, Terayama K, Wong JS, Vale RD, Walter P, Farese RV. Functional genomic screen reveals genes involved in lipid-droplet formation and utilization. *Nature.* 2008;453(7195):657–61.
- Krahmer N, Guo Y, Wilfling F, Hilger M, Lingrell S, Heger K, Newman HW, Schmidt-Supprian M, Vance DE, Mann M, et al. Phosphatidylcholine synthesis for lipid droplet expansion is mediated by localized activation of CTP:phosphocholine cytidylyltransferase. *Cell Metab.* 2011;14(4):504–15.
- Hou XH, Zhang R, Yang M, Niu NQ, Wu JC, Shu Z, Zhang PF, Shi LJ, Zhao FP, Wang LG, et al. Metabolomics and lipidomics profiles related to intramuscular fat content and flavor precursors between Laiwu and Yorkshire pigs. *Food Chem.* 2023;404:134699.
- Čopič A, Dieudonné T, Lenoir G. Phosphatidylserine transport in cell life and death. *Curr Opin Cell Biol.* 2023;83:102192.
- Leventis PA, Grinstein S. The distribution and function of phosphatidylserine in cellular membranes. *Annu Rev Biophys.* 2010;39:407–27.
- Zhou JW, Zhang Y, Wu JJ, Qiao M, Xu Z, Peng XW, Mei SQ. Proteomic and lipidomic analyses reveal saturated fatty acids, phosphatidylinositol, phosphatidylserine, and associated proteins contributing to intramuscular fat deposition. *J Proteomics.* 2021;241:104235.
- Dudek J, Hartmann M, Rehling P. The role of mitochondrial cardiolipin in heart function and its implication in cardiac disease. *BBA-Mol Basis Dis.* 2019;1865(4):810–21.
- Houtkooper RH, Vaz FM. Cardiolipin, the heart of mitochondrial metabolism. *Cell Mol Life Sci.* 2008;65(16):2493–506.
- Mendham AE, Goedecke JH, Zeng YX, Larsen S, George C, Hauksson J, Fortuin-de Smidt MC, Chibalin AV, Olsson T, Chorell E. Exercise training improves mitochondrial respiration and is associated with an altered intramuscular phospholipid signature in women with obesity. *Diabetologia.* 2021;64(7):1642–59.
- Hannun YA, Obeid LM. Sphingolipids and their metabolism in physiology and disease. *Nat Rev Mol Cell Bio.* 2018;19(3):175–91.
- Zhang R, Yang M, Hou XH, Hou RD, Wang LG, Shi LJ, Zhao FP, Liu X, Meng QS, Wang LX, et al. Characterization and difference of lipids and metabolites from Jianhe White Xiang and Large White pork by high-performance liquid chromatography-tandem mass spectrometry. *Food Res Int.* 2022;162:111946.
- Adhikari M, Kantar MB, Longman RJ, Lee CN, Oshiro M, Caires K, He YH. Genome-wide association study for carcass weight in pasture-finished beef cattle in Hawai'i. *Front Genet.* 2023;14:1168150.

Publisher's Note

Springer Nature remains neutral with regard to jurisdictional claims in published maps and institutional affiliations.